Electronic Supplementary Material (ESI)

Synergistic Effect of Atomically Dual-metal Doped Catalyst for Highly Efficient Oxygen Evolution

Daobin Liu[a‡], Shiqing Ding[a‡], Chuanqiang Wu[a], Wei Gan[ad], Changda Wang[a], Dengfeng Cao[a], Zia ur Rehman[a], Yuan Sang[a], Shuangming Chen[a*], Xusheng Zheng[a], Yu Wang[c], Binghui Ge[b], Li Song[a*]

[a] National Synchrotron Radiation Laboratory, Department of chemical physics, CAS Center for Excellence in Nanoscience, University of Science and Technology of China. Hefei, Anhui 230026, China

[b] Beijing National Laboratory for Condensed Mater Physics, Institute of Physics, Chinese Academy of Sciences, Beijing 100190, China

[c] Shanghai Synchrotron Radiation Facility, Shanghai Institute of Applied Physics, Chinese Academy of Sciences, Shanghai 201204, China

[d] Institute for Frontier Materials, Deakin University, Geelong Waurn Ponds Campus, Waurn Ponds, VIC 3216, Australia

*Corresponding author: csmp@ustc.edu.cn (S. Chen); song2012@ustc.edu.cn (L. Song)

‡ These authors contributed equally to this work.

Experimental Section

Preparation of the NiFe@g-C_3N_4/CNT catalyst.

Multi-walled carbon nanotubes (MWCNTs) (Nanjing XFNANO Materials Tech Co., Ltd) were first purified and oxidized according to the previous report. Typically, 1g CNT was calcined at 350 ºC for 1h in the air, and washed with dilute HCl for several times to eliminate metal impurities. After drying, the oxidized CNT was added to 23 mL concentrated H_2SO_4 and stirred for 20 h at room temperature. Then 350 mg of $NaNO_3$ were added, followed by slow addition of 1 g of $KMnO_4$ at 40 ℃ in a water bath. The mixture was stirred for 30 min and 3 mL of water were added, followed by another 3 mL of water after 5 min. After another 5 min, 40 mL of water were added, followed by stirring for 15 min. The solution was removed from water bath and 140 mL of water and 10 mL of 30% H_2O_2 were added. Finally, the mildly oxidized CNT were collected, washed repeatedly with diluted HCl and water and dried it.

250 mg dicyandiamide (DCDA) was dissolved in 32 mL deionized water, and then added 4 mL $NiCl_2$ $6H_2O$ (0.0125 M) and 4 mL $FeCl_3$ $6H_2O$ (0.0125 M) solution. Then it was stirred at 80 ℃ for 3 h. After cooling to the room temperature, 1.25 g NH_4Cl and 120 mg the oxidized CNT was added into the solution, combined with sonication to get homogeneous dispersion, and followed by lyophilization to dry it. The obtained powder was treated at 550 ºC with a ramp rate of 2.3 ºC min^{-1} for 4h in N_2 atmosphere (denoted as NiFe@g-C_3N_4/CNT). For comparison, preparation of the single-metal doped catalyst (Ni@g-C_3N_4/CNT and Fe@g-C_3N_4/CNT) and the hybrid without NH_4Cl (NiFe@g-C_3N_4/CNT_w/o NH_4Cl) were the same as NiFe@g-C_3N_4/CNT, except the raw materials were without the addition of $FeCl_3$ $6H_2O$, $NiCl_2$ $6H_2O$ and NH_4Cl, respectively. Note that the amounts of metal precursors in these hybrids were consistent with that of NiFe@g-C_3N_4/CNT. The g-C_3N_4/CNT hybrid was prepared using DCDA, MWCNTs and NH_4Cl as precursors without metal salts.

Characterizations

Transmission electron microscopy (TEM) and high-resolution TEM images were collected on a JEM-2100F field emission electron microscope at an accelerating voltage of 200 kV. Aberration-corrected high-angle annular dark-field scanning transmission electron microscopy (HAADF-STEM) measurements and energy dispersive X-ray spectra (EDS)-mapping images,

using a 200 kV JEM-ARM200F equipped with double spherical aberration correctors. Field emission scanning electron microscopy (FESEM) images were taken on a JEOL JSM-6700F SEM. The PerkinElmer Optima 7300 DV ICP-AES instrument was used to determine the metal loading content after digesting the as-obtained sample in HNO_3. X-ray diffraction (PXRD) patterns were obtained using a Japan Rigaku DMax-γA rotation anode X-ray diffractometer equipped with graphite monochromatized Cu Kα radiation (λ = 1.54178 Å). X-ray photoelectron spectroscopy (XPS) spectra was measured on a Thermal Fisher ESCALAB250Xi spectrometer equipped with an Al anode (Al K_α= 1486.7 eV). The N_2 adsorption-desorption experiments were carried out using Micromeritics ASAP 2020 instrument. XAFS spectra were collected at MCD endsation in the National Synchrotron Radiation Laboratory (NSRL), the beamline 14W1 in Shanghai Synchrotron Radiation Facility (SSRF) and the beamline 1W1B in the Beijing Synchrotron Radiation Facility (BSRF).The acquired EXAFS data were fit using the FEFF8.2 code.

Electrochemical measurements

Typically, 5 mg of catalyst was first dispersed in 1 mL solution (water/isoproparol = 1:1, v/v) and sonicated to obtain a homogeneous ink, followed by the addition of 50 μL 5 wt.% Nafion solution (the amount of binder has little influence on the catalyst conductivity and the intrinsic OER performance). A certain amount of the ink was deposited on the polished glassy carbon electrode (different diameter of glassy carbon disk in rotating disk electrode (RDE) (5.0 mm) and rotating ring-disk electrode (RRDE) (5.61 mm), normalized to the loading area with 0.382 mg cm^{-2}) and dried at room temperature. All electrochemical measurements were performed on the CHI760E (CH Instruments, China) electrochemical workstation with a standard three-electrode setup. A graphite rod and saturated Ag/AgCl served as the counter and reference electrodes, respectively. All potentials were calibrated to the reversible hydrogen electrode ($E_{RHE} = E_{Ag/AgCl} + 1.025$ V), and all polarization curves were without iR compensation.

RDE measurements were performed in O_2-saturated 1 M KOH electrolyte from 1 to 1.8 V (vs. RHE) with a speed of 1600 rpm and a scan rate of 5 mV s^{-1}. Electrochemical impedance spectroscopy (EIS) measurements were carried out at an overpotential of η=350 mV, from 10^5 to 0.1 Hz, with an AC amplitude of 5 mV. Cyclic voltammetry were conducted between 0.925 and 1.125 V (vs. RHE) from 5 to 100 mV s^{-1} in order to investigate the electrochemical active surface

area (ECSA) of catalysts. The stability of NiFe@g-C_3N_4/CNT was evaluated using 3,000 continuous cycles from 1.2 to 1.6 V (vs. RHE) in O_2-saturated 1M KOH at a scan rate of 100 mV s^{-1}, and the chronopotentiometry method at the current density of 10 mA cm^{-2} for 18h. Note that the catalyst was loaded onto carbon paper with the area of 1 cm^2 (Toray, TGP-H-60) for stability test.

To detect the production of H_2O_2, the rotating ring-disk electrode (RRDE) measurements were conducted in N_2-saturated 1 M KOH electrolyte from 1 to 1.8 V (vs. RHE) with a speed of 1600 rpm and a scan rate of 5 mV s^{-1}, and the Pt-ring electrode potential was set to 1.4 V (vs. RHE). The Faradaic efficiency was calculated by the equation of $I_{ring}/(NI_{disk})$ (where I_{ring} and I_{disk} are the current response of Pt-ring and disk electrode, respectively, and N is the collection efficiency of the RRDE which was determined to be ~0.37), and the corresponding experiments were performed under the same conditions, except that the disk current was maintained at 480 μA and the Pt-ring electrode potential was set to 0.5 V (vs. RHE) to reduce the formation of O_2.

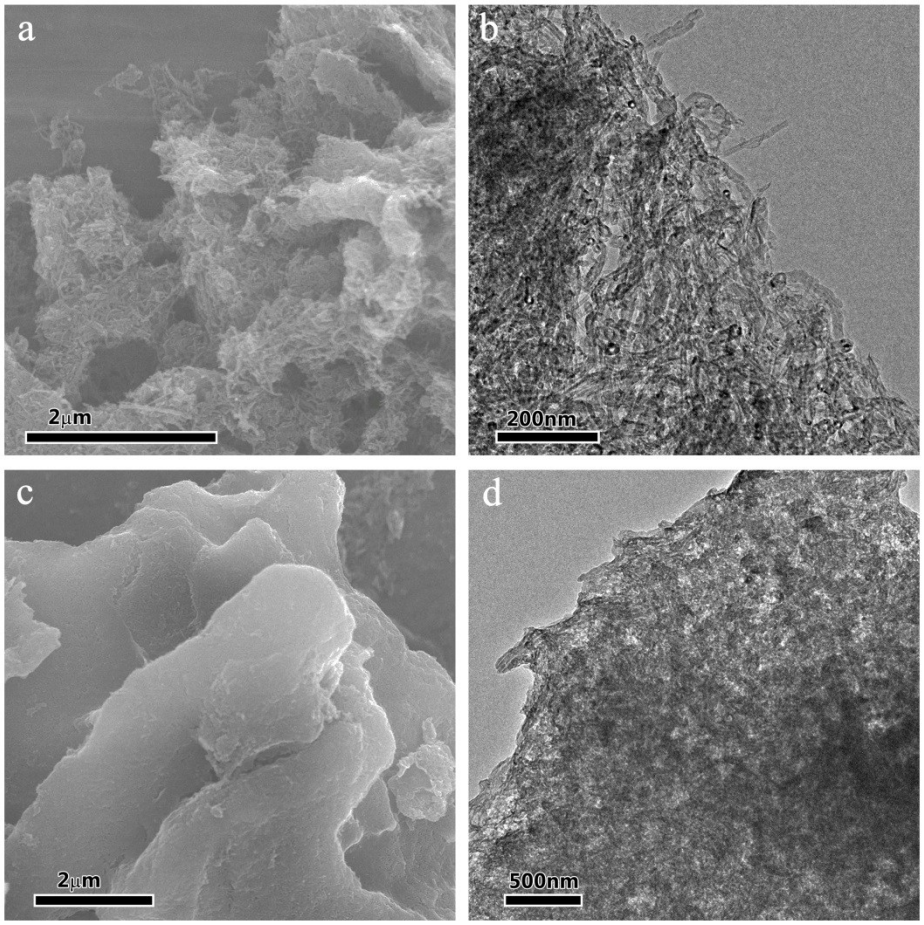

Fig. S1 (a) and (c) FESEM images, (b) and (d) TEM images of NiFe@g-C_3N_4/CNT and NiFe@g-C_3N_4/CNT_w/o NH_4Cl, respectively.

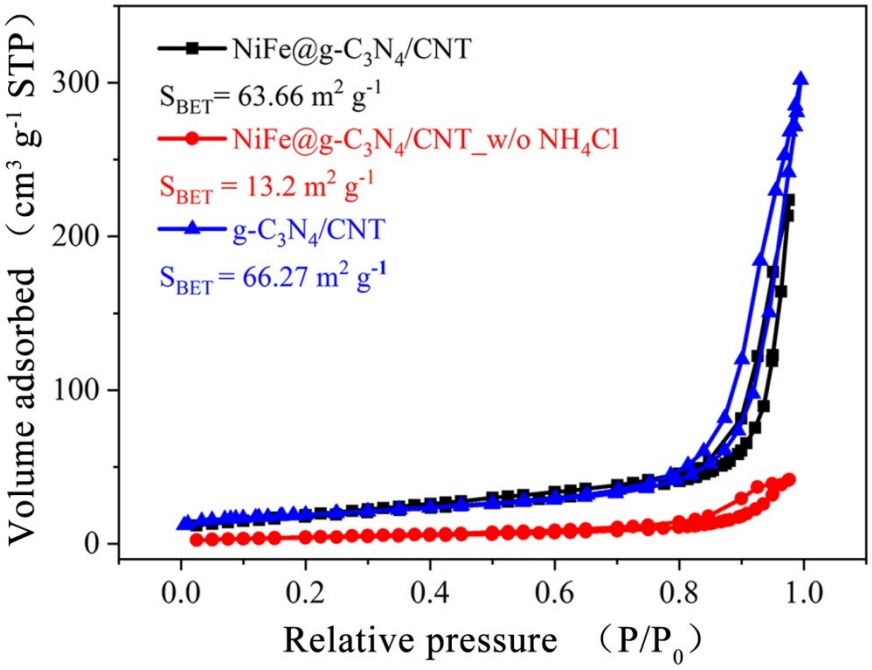

Fig. S2 Nitrogen adsorption-desorption isotherm of NiFe@g-C_3N_4/CNT, NiFe@g-C_3N_4/CNT_w/o NH_4Cl and g-C_3N_4/CNT.

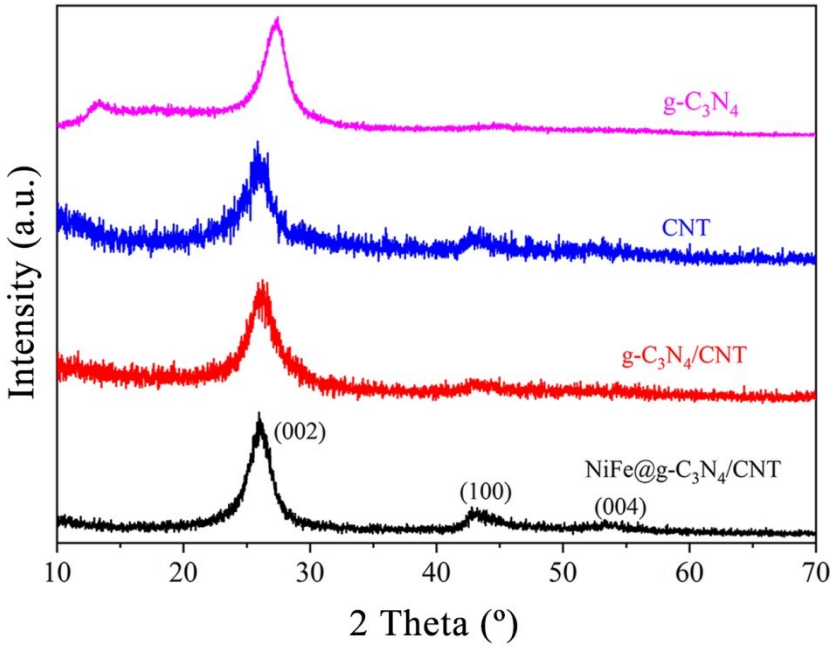

Fig. S3 XRD patterns of NiFe@g-C_3N_4/CNT, g-C_3N_4/CNT, CNT and C_3N_4, where showed no additional peaks corresponding metal nanoparticles.

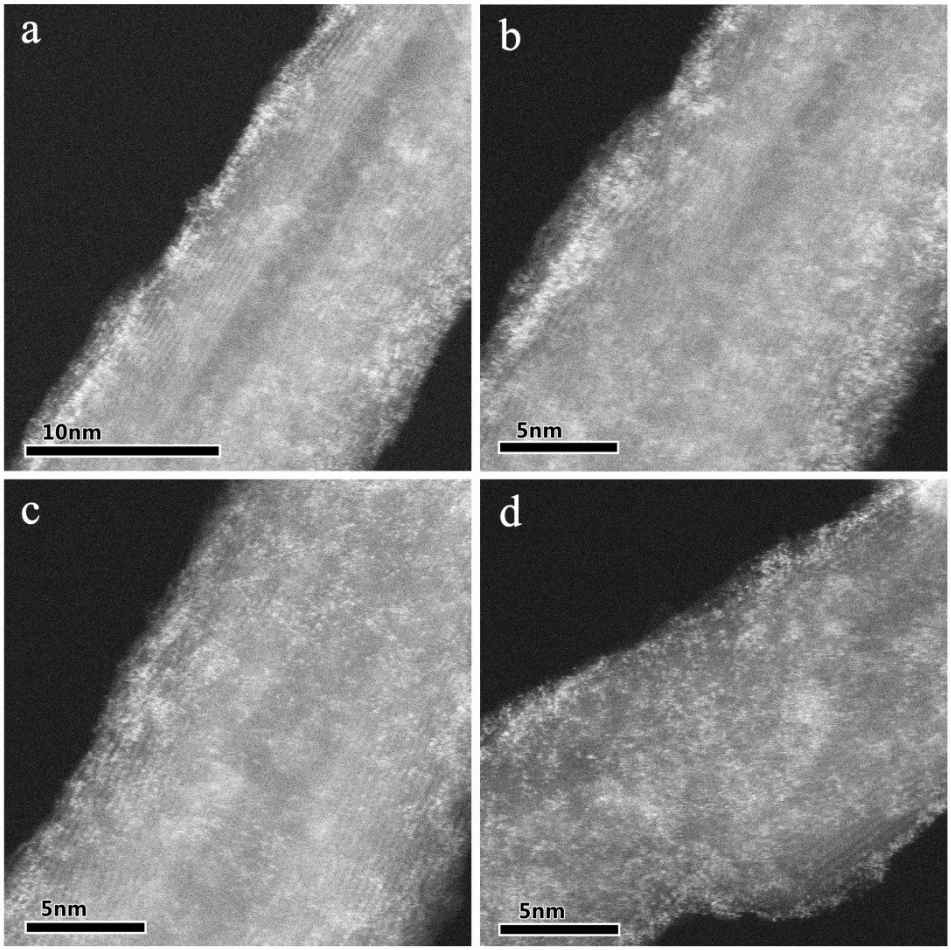

Fig. S4 HAADF-STEM images of NiFe@g-C_3N_4/CNT in different region, indicating that Ni/Fe atoms were anchored on g-C_3N_4/CNT supports without any aggregations.

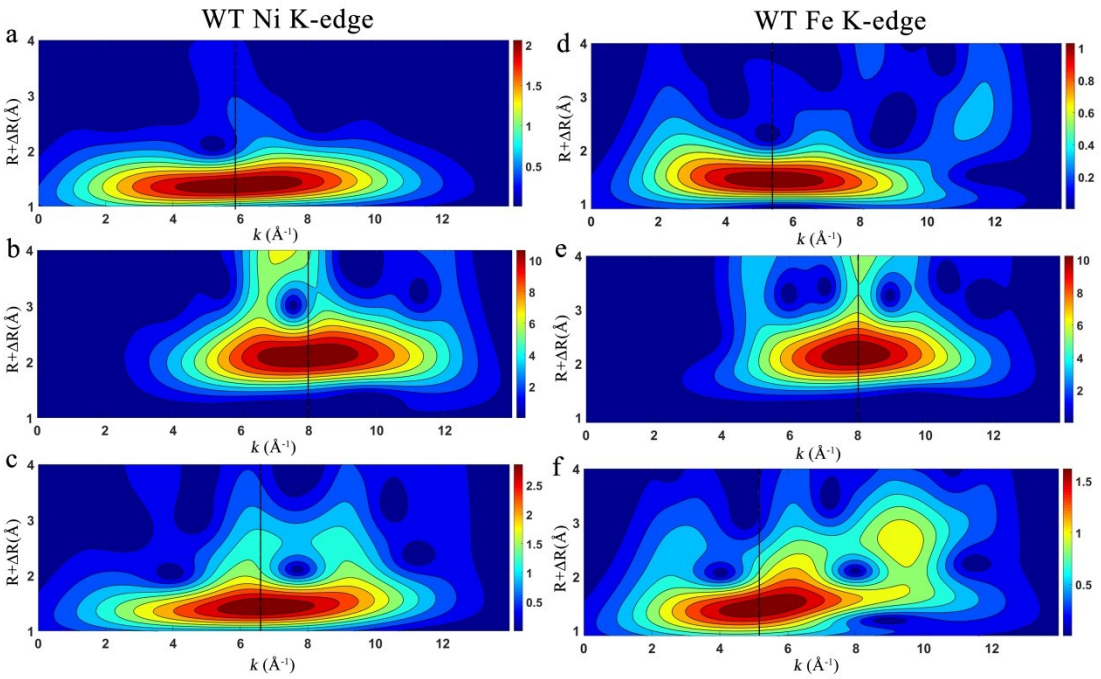

Fig. S5 Wavelet transform (WT) Ni K-edge EXAFS spectra of (a) NiFe@g-C_3N_4/CNT, (b) Ni foil and (c) NiPc. And WT Fe K-edge EXAFS spectra of (d) NiFe@g-C_3N_4/CNT, (e) Fe foil and (f) FePc.

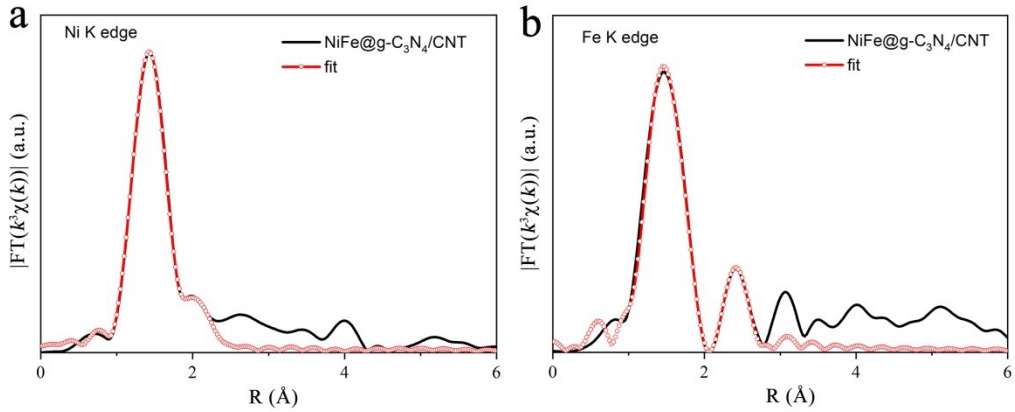

Fig. S6 The corresponding R space fitting curve of NiFe@ g-C_3N_4/CNT at Ni K-edge (a) and Fe K-edge (b).

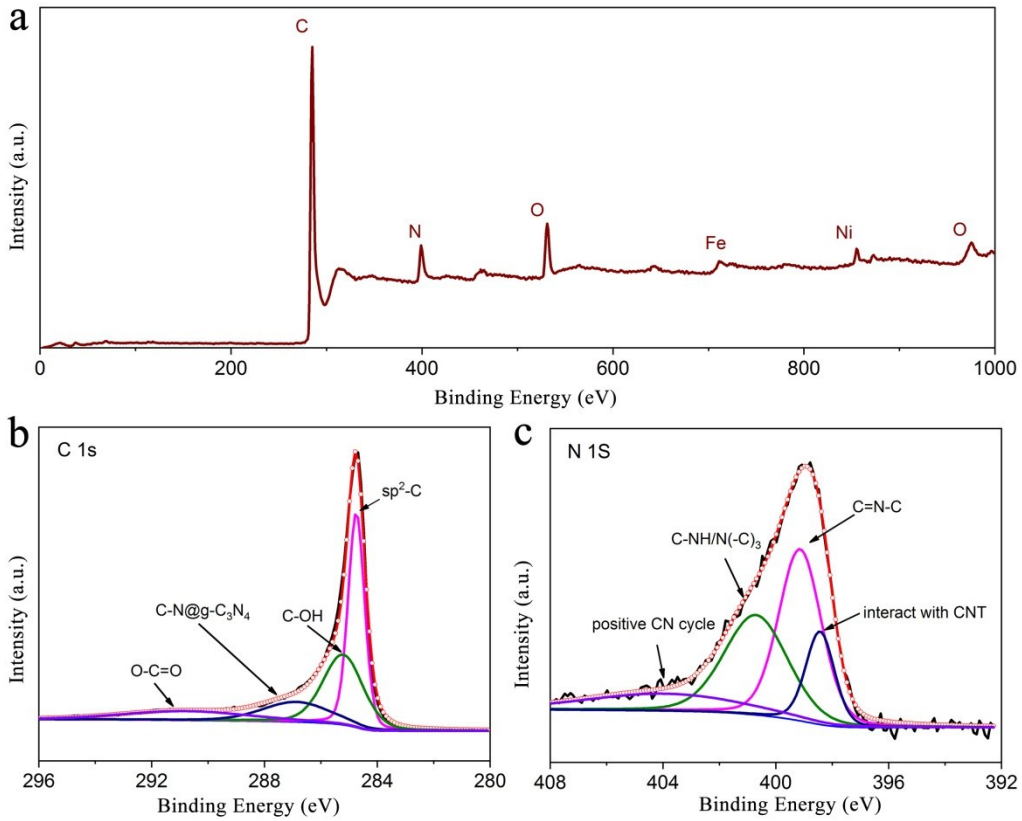

Fig. S7 The XPS survey (a), C 1s (b) and N 1s (c) high-resolution spectra of NiFe@ g-C_3N_4/CNT.

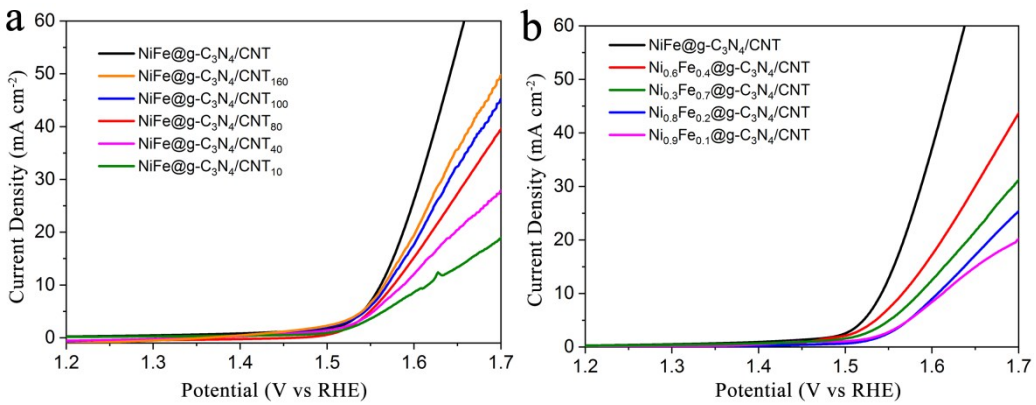

Fig. S8 Typical polarization curves of as-prepared hybrids with different ratio of DCDA/CNT (a) and Ni/Fe species (b).

The result in Fig. S8a reveals that the OER activity was enhanced with the increase of CNT content but dramatically decreased in NiFe@g-C_3N_4/CNT_{160}, because of the relatively low proportion of active NiFe@g-C_3N_4. It confirmed that CNT skeletons play an important role of conductive additive to accelerate the electron transfer in catalytic process. Fig. S8b clearly shows that the trend of apparent OER activity resembles the "volcano curve" by altering the Ni/Fe ration in as-prepared hybrids. The NiFe@g-C_3N_4/CNT hybrid has a better OER activity compared to that of other hybrids. The catalytic performance was delayed with an excessive Fe species, resulting from the relatively low Ni sites in high oxidation states.

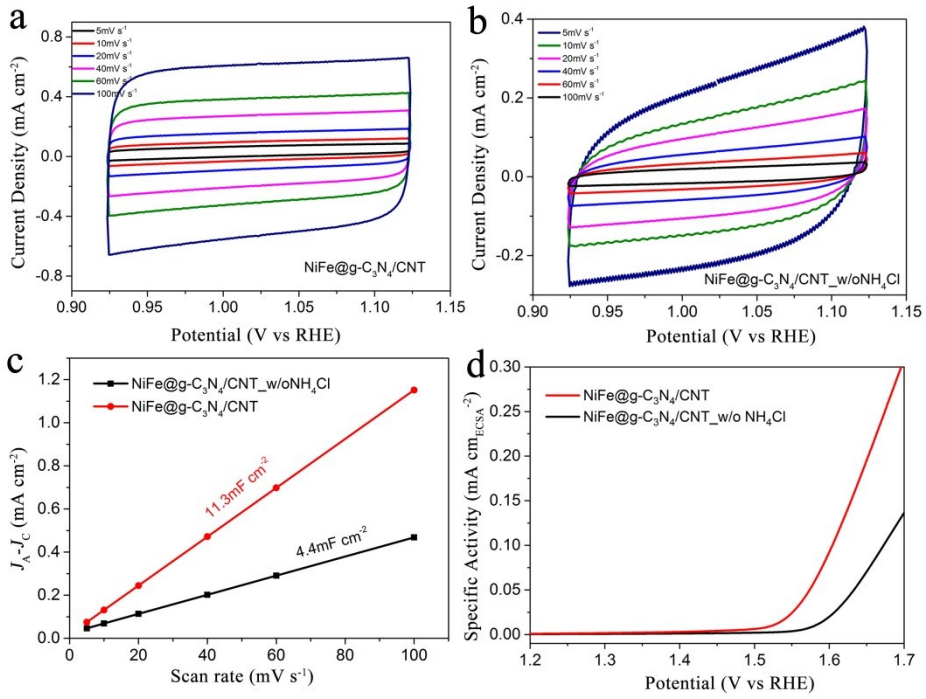

Fig. S9 CVs of NiFe@ g-C_3N_4/CNT (a) and NiFe@g-C_3N_4/CNT_w/o NH_4Cl (b) measured in non-Faradaic region at different scan rate. (c) The current difference was calculated at 1.125 V (vs. RHE) as a function of scan rate. (d) Specific activity of NiFe@g-C_3N_4/CNT and NiFe@g-C_3N_4/CNT w/o NH_4Cl was normalized by ECSA.

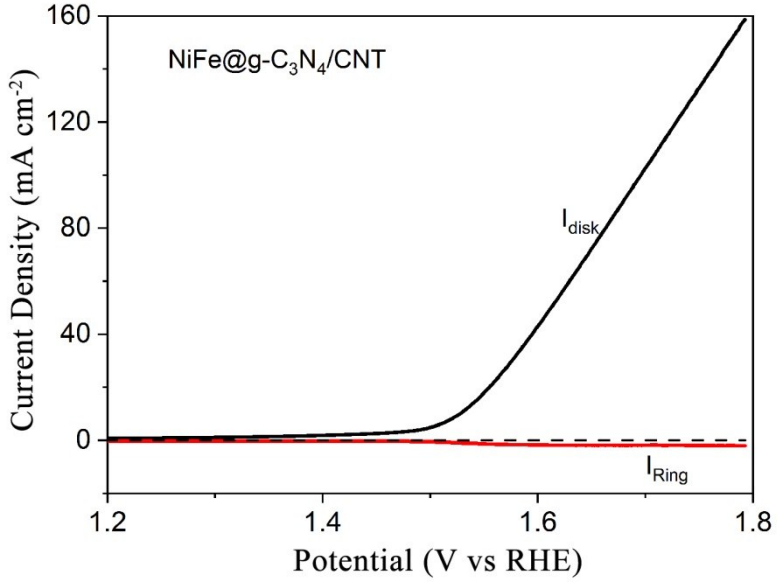

Fig. S10 The detection of H_2O_2 production by RRDE measurement (Ering= 1.40 V).

Table S1 Ni K-edge structural parameters of NiFe@g-C_3N_4/CNT and the reference NiPc and Fe foil materials extracted from quantitative EXAFS fitting curves (σ^2 is Debye-Waller factor).

		N (coordination number)	Bond length	$\sigma^2(10^{-3}$ Å$^2)$
NiFe@g-C_3N_4/CNT	Ni-N_1	3.2	1.86	6.9
	Ni-O	1.0	2.08	7.3
	Ni-Ni	0.6	2.49	9.2
NiPc	Ni-N_1	4	1.89	4.8
	Ni-O	2	2.12	6.5
	Ni-C	8	2.76	11.1
	Ni-N_2	4	3.18	7.8
Ni foil	Ni-Ni	8	2.48	6.2

Note: Ni-N_1 and Ni-N_2 showing in the table represents the nearest and the next nearest Ni-N coordination.

Table S2 Fe K-edge structural parameters of NiFe@g-C_3N_4/CNT and the reference NiPc and Fe foil materials extracted from quantitative EXAFS fitting curves (σ^2 is Debye-Waller factor).

		N (coordination number)	Bond length	$\sigma^2(10^{-3}$ Å$^2)$
NiFe@g-C_3N_4/CNT	Fe-N_1	3.5	1.96	5.1
	Fe-O	1.2	2.05	3.6
	Fe-C	4.1	2.87	3.3
	Fe-Fe	0.3	2.89	9.7
FePc	Fe-N_1	4	2.01	4.8
	Fe-O	2	2.04	3.2
	Fe-C	8	3.01	1.6
	Fe-N_2	4	3.39	9.9
Fe foil	Fe-Fe	8	2.46	5.0
	Fe-Fe	6	2.83	5.0

Note: Fe-N_1 and Fe-N_2 showing in the table represents the nearest and the next nearest Fe-N coordination.

Table S3 Comparison of OER performance in alkaline with other metal-free catalysts and carbon-based catalysts coupled with metal-N_x structure.

Catalyst	Tafel slope (mV dec^{-1})	η @10 mA cm^{-2} (mV)	Electrolyte	Ref.
CNNTS	383	450	0.1 M KOH	[S1]
Co_4N/CNW/CC	81	330	1 M KOH	[S2]
Co/N-CNTs	67	390	0.1 M KOH	[S3]
S,N-Fe/N/C-CNT	82	370	0.1 M KOH	[S4]
OCC-8	82	492	0.1 M KOH	[S5]
Co-C_3N_4/CNT	68.4	380	0.1 M KOH	[S6]
N-GRW	47	360	1 M KOH	[S7]
g-C_3N_4 and CNTs	83	350	0.1 M KOH	[S8]
N/C	--	380	0.1 M KOH	[S9]
NiFe@g-C_3N_4/CNT	67	326	1 M KOH	This work

Reference

1. R. M. Yadav, J. Wu, R. Kochandra, L. Ma, C. S. Tiwary, L. Ge, G. Ye, R. Vajtai, J. Lou and P. M. Ajayan, *ACS. Appl. Mater. Inter.*, 2015, **7,** 11991-12000.
2. F. Meng, H. Zhong, D. Bao, J. Yan and X. Zhang, *J. Am. Chem. Soc.*, 2016, **138**, 10226-10231.
3. Y. Liu, H. Jiang, Y. Zhu, X. Yang and C. Li, *J. Mater. Chem. A*, 2016, **4**, 1694-1701.
4. P. Chen, T. Zhou, L. Xing, K. Xu, Y. Tong, H. Xie, L. Zhang, W. Yan, W. Chu, C. Wu and Y. Xie, *Angew. Chem. Int. Ed.*, 2017, **56**, 610-614.
5. N. Cheng, Q. Liu, J. Tian, Y. Xue, A. M. Asiri, H. Jiang, Y. He and X. Sun, *Chem. Commun.*, 2015, **51**, 1616-1619.
6. Y. Zheng, Y. Jiao, Y. Zhu, Q. Cai, A. Vasileff, L. H. Li, Y. Han, Y. Chen and S. Z. Qiao, *J. Am. Chem. Soc.*, 2017, **139**, 3336-3339.
7. H. B. Yang, J. Miao, S. F. Hung, J. Chen, H. B. Tao, X. Wang, L. Zhang, R. Chen, J. Gao, H. M. Chen, L. Dai and B. Liu, *Sci. Adv.*, 2016, **2**, e1501122.
8. T. Y. Ma, S. Dai, M. Jaroniec, S. Z. Qiao, *Angew. Chem. Int. Ed.*, 2014, **53**, 7281-7285.
9. Y. Zhao, R. Nakamura, K. Kamiya, S. Nakanishi and K. Hashimoto, *Nat. Commun.*, 2013, **4**, 2390.